PHYSICAL REVIEW FLUIDS **1**, 082301(R) (2016)

Boundary layer fluctuations and their effects on mean and variance temperature profiles in turbulent Rayleigh-Bénard convection

Yin Wang,[1] Xiaozhou He,[2] and Penger Tong[1]

[1]*Department of Physics, Hong Kong University of Science and Technology, Clear Water Bay, Kowloon, Hong Kong, China*

[2]*Institute for Turbulence-Noise-Vibration Interaction and Control, Shenzhen Graduate School, Harbin Institute of Technology, Shenzhen, China*

(Received 1 February 2016; published 9 December 2016)

We report simultaneous measurements of the mean temperature profile $\theta(z)$ and temperature variance profile $\eta(z)$ near the lower conducting plate of a specially designed quasi-two-dimensional cell for turbulent Rayleigh-Bénard convection. The measured $\theta(z)$ is found to have a universal scaling form $\theta(z/\delta)$ with varying thermal boundary layer (BL) thickness δ, and its functional form agrees well with the recently derived BL equation by Shishkina *et al.* [Phys. Rev. Lett. **114**, 114302 (2015)]. The measured $\eta(z)$, on the other hand, is found to have a scaling form $\eta(z/\delta)$ only in the near-wall region with $z/\delta \lesssim 2$. Based on the experimental findings, we derive a BL equation for $\eta(z/\delta)$, which is in good agreement with the experimental results. These BL equations thus provide a common framework for understanding the effect of BL fluctuations.

DOI: 10.1103/PhysRevFluids.1.082301

I. INTRODUCTION

Turbulent Rayleigh-Bénard convection (RBC) is a classical model used to study turbulent thermal convection, which can be found in many natural processes and industrial applications [1–6]. In the laboratory RBC is realized in a confined fluid layer, which is heated from below and cooled from the top with a vertical temperature gradient parallel to gravity. As a wall-bounded flow, RBC has the temperature and velocity boundary layers (BLs) adjacent to the upper and lower conducting plates. The structure and dynamics of the temperature BL are of great importance, as they determine the global heat transport of the system. When the Rayleigh number Ra (dimensionless buoyancy) is moderate, the normalized mean temperature profile $\theta(z)$ was assumed to be laminar [7] and to have the Prandtl-Blasius-Pohlhausen (PBP) form [8,9]. Here z is the vertical distance away from the conducting plate. As Ra becomes sufficiently large, the BLs are expected to transit into a turbulent state due to the shear instability caused by the bulk flow [10]. In this regime, $\theta(z)$ was predicted to follow a logarithmic profile [11–13].

In fact, there is a large class of BL flows remaining in the transition regime between the laminar and fully turbulent states. The thermal BL in turbulent Rayleigh-Bénard convection with $\mathrm{Ra} \lesssim 10^{14}$ (above which the BL becomes turbulent) is an example of such flows, in which the BL is not fully turbulent yet but there are significant BL fluctuations resulting from intermittent eruption of thermal plumes from the BL. Recent studies in the system with convection cells of different shape, ranging from rectangular and cubic to cylindrical, showed [14–28] that the measured (and numerically calculated) $\theta(z)$ has a universal form $\theta(\xi)$ independent of Ra in a wide dynamic range of $10^8 \lesssim \mathrm{Ra} \lesssim 10^{12}$, where $\xi \equiv z/\delta$ is the vertical distance from the conducting plate normalized by the thermal BL thickness δ. The measured $\theta(\xi)$ was found to have the PBP form only when ξ is in the region $\xi \lesssim 0.6$ [16,17,20]. Deviations of $\theta(\xi)$ from the PBP form were found when $0.6 \lesssim \xi \lesssim 4$ [16,19,23–25]. The deviations were attributed to BL fluctuations and they still exist after a dynamical rescaling method was applied to the measured $\theta(z)$ [18,29]. When $\xi \gtrsim 8$, a logarithmic layer was found, where $\theta(z)$ changes logarithmically with z [30–32].

An important issue that has not been resolved in the earlier studies is what exactly causes the deviations and how to mathematically describe these deviations. More recently, Shishkina *et al.* [33]

considered the effect of BL fluctuations and included the velocity-temperature correlation function $\langle v'T'\rangle$ in the two-dimensional BL equation for $\theta(z)$, where T' and v' are, respectively, the local temperature and vertical velocity fluctuations and $\langle\cdots\rangle$ denotes an average over time t. Under the assumptions that the thermal BL is nested underneath the velocity BL and that $\langle v'T'\rangle = -\kappa_t\partial_z\langle T\rangle$ with the turbulent thermal diffusivity $\kappa_t \simeq a^3\xi^3\kappa$, where κ is the thermal diffusivity of the convecting fluid and a is a numerical constant, Shishkina *et al.* obtained an analytical form of the mean temperature profile [33]

$$\theta(\xi;c) \equiv \frac{T_b - \langle T(\xi)\rangle}{\Delta_b} = \int_0^\xi (1+a^3\eta^3)^{-c}d\eta, \tag{1}$$

where $\Delta_b \equiv T_b - T_0$ is the temperature difference across the BL with T_b and T_0 being, respectively, the temperature of the bottom plate and at the cell center. In the above, $c \geqslant 1$ is a parameter that satisfies the condition $a = \Gamma(1/3)\Gamma(c-1/3)/3\Gamma(c)$. When $c \to \infty$, $\theta(\xi;\infty)$ approaches the PBP form for laminar BLs without BL fluctuations.

Equation (1) was tested only with the direct numerical simulation (DNS) data [33]. While there exit a number of experimental studies of the mean temperature profile $\theta(z)$ in turbulent convection [14–17,19,20], most of the experiments were conducted under conditions different from those specified for Eq. (1). Some of the experiments [14,15,19] were conducted in air (or in a gas) with the Prandtl number $\mathrm{Pr} = \nu/\kappa \simeq 0.7$, where ν is the kinematic viscosity of the convecting fluid. In this case, the thermal BL is no longer nested underneath the velocity BL. For those experiments with $\mathrm{Pr} > 1$ [16,17,20], many of them were conducted in upright cylindrical cells, in which the large-scale flow is not two dimensional and has several three-dimensional (3D) flow modes, such as torsional and sloshing oscillations [34–36]. There are also corner flows in the closed cylinder [37], which may destabilize the large-scale flow [38,39]. The strong coupling between the BL dynamics and complex 3D large-scale flow in a closed cylinder, which has been studied in recent numerical simulations [18,21–27], makes a quantitative comparison between the theory and experiment difficult.

In this Rapid Communication we report direct measurements of the mean temperature profile $\theta(z)$ and temperature variance profile $\eta(z) \equiv \langle[T(z,t) - \langle T(z)\rangle]^2\rangle$ near the lower conducting plate of a specially designed quasi-two-dimensional cell for turbulent Rayleigh-Bénard convection. The measured $\theta(z)$ is found to have a universal scaling form $\theta(z/\delta)$, which is well described by Eq. (1) and the value of the fitting parameter c is found to change sensitively with Pr. The measured $\eta(z)$, on the other hand, is found to have a scaling form $\eta(\xi)$ only in the near-wall region with $\xi \lesssim 2$. For $\xi > 2$, the measured $\eta(z)$ for different values of Ra scales with z/D, where D is the diameter of the cell. This result suggests that a different characteristic length takes over the dynamics in this region. Based on the experimental findings, we derive a BL equation for $\eta(\xi)$ with $\mathrm{Pr} > 1$ and obtain a numerical solution of $\eta(\xi)$, which is in excellent agreement with the experimental data.

II. EXPERIMENT

The convection experiment is conducted in a vertical thin disk with its circular cross section aligned parallel to gravity. As shown in Fig. 1(a), the cell has a diameter $D = 188$ mm and thickness $W = 20$ mm and thus the corresponding aspect ratio $\Gamma \equiv W/D = 0.11$. The top and bottom thirds of the circular sidewall are made of copper of 8 mm in thickness. The surface of the copper plates in contact with the convecting fluid is electroplated with a thin layer of nickel. The remaining third of the sidewall on both sides is made of transparent Plexiglas 18 mm in thickness. The two flat end walls of the cell are also made of the same type of Plexiglas. Two silicon rubber film heaters connected in parallel are sandwiched on the back side of the bottom conducting plate to provide constant and uniform heating. The top copper plate is in contact with a cooling chamber consisting of two water channels. The temperature of the top plate is maintained by a temperature-controlled circulator (NESLAB, RTE740), which circulates the cooling water with a temperature stability of 10 mK. The temperature of the top and bottom plates is measured at a rate of 2 Hz by the calibrated

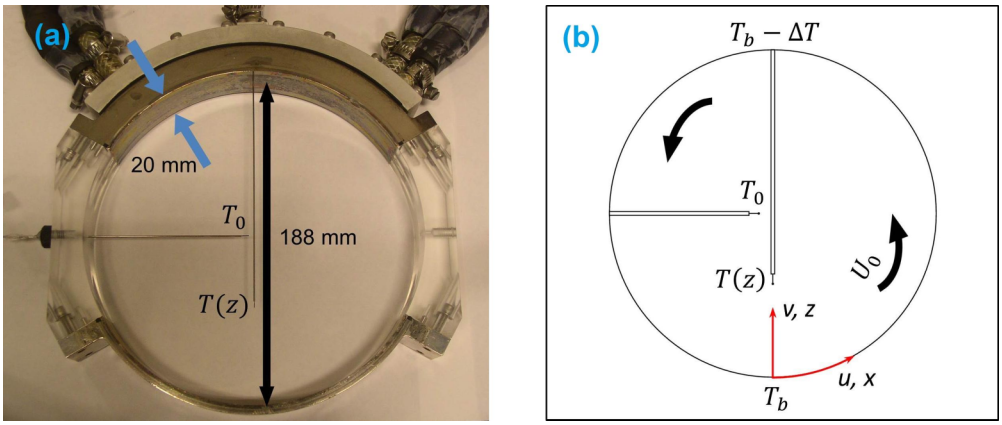

FIG. 1. (a) End view of the actual convection cell used in the experiment. The temperature T_0 at the cell center and the temperature profile $T(z)$ along the vertical axis of the cell are measured using two movable thermistors. (b) Sketch of the experiment setup for the measurement of the local temperature profiles near the lower conducting plate. The black arrows indicate the direction of the large-scale flow of speed U_0 in the circular cross section of the cell. The red arrows indicate the velocity components and spatial coordinates used in the experiment.

thermistors with an accuracy of 5 mK. They are embedded in each plate at 1 mm away from the surface of the conducting plate. This cell was used in an early convection experiment [40].

The cell has a circular cross section without any corner in order to prevent secondary flows. The large-scale flow in the circular cross section of the cell has a flywheel-like structure with a mean rotating speed U_0 along a fixed orientation (counterclockwise). The velocity components and spacial coordinates used in the experiment are indicated in Fig. 1(b). Because the flow is confined in a thin circular disk, no other flow modes can be excited in this quasi-2D system. Compared with the large-scale flow in a conventional upright cylinder, this quasi-2D flow has a better geometry satisfying the assumption of the boundary layer theory for a 2D flow over an infinite horizontal plane. These simplifications allow us to have a stringent test of the theory. In this system, the Rayleigh number is defined as $\mathrm{Ra} \equiv \psi g \Delta T D^3/\nu\kappa$, where g is the gravitational acceleration, ΔT is the temperature difference between the two copper surfaces, and ψ is the thermal expansion coefficient of the working fluid. In the experiment, Ra is varied in the range $1.5 \times 10^9 \lesssim \mathrm{Ra} \lesssim 1.3 \times 10^{10}$ and the Prandtl number Pr is fixed. Two working fluids are used: One is distilled water (with $\mathrm{Pr} = 4.4$) and the other is a 20 wt.% aqueous solution of glycerin ($\mathrm{Pr} = 7.6$).

The local fluid temperature is measured using two glass-encapsulated thermistors with a diameter of 0.17 mm and a time constant of 10 ms (AB6E3- B05KA202R, Thermometrics). One thermistor is movable along the central vertical axis of the cell to measure $T(z)$, and the other thermistor is placed at the cell center to measure T_0. Details about the temperature calibration and measurements have been reported elsewhere [41]. To guide the two thermistors into the convection cell, we install horizontal and vertical stainless steel tubes on the sidewall, as shown in Fig. 1. The stainless steel tube (type 304 SS hypodermic tubing, 19 Ga, McMASTER-CARR) has an outer diameter of 1.1 mm and wall thickness of 0.19 mm. Thin wires of each thermistor thread through a tube from the inside and the small thermistor bead is kept outside of the tube end in the cell. In the experiment, the horizontal tube is fixed to measure the temperature T_0 at the cell center. The vertical tube is used to measure the vertical temperature profile $T(z)$ along the central axis of the cell and is mounted on a translational stage, which is controlled by a stepping motor with a position resolution of 50 μm. The measurements of T_0 and $T(z)$ are made, respectively, at rates of 2 and 15 Hz. The accuracy of the temperature measurement is 5 mK.

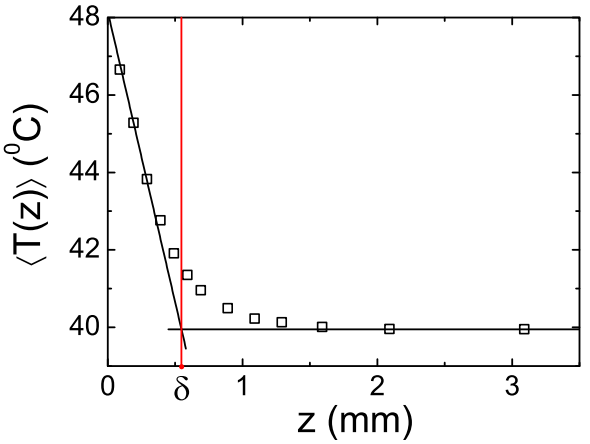

FIG. 2. Measured mean temperature profile $\langle T(z)\rangle$ as a function of distance z away from the bottom conducting plate for water (Pr = 4.4) at Ra = 4.23×10^9. The vertical red line indicates the thermal BL thickness δ, which is determined from the intersection position between the two black lines.

Recent studies [40,42] have revealed that this system possesses the key features of turbulent convection, which have been observed in the upright cylinders. In particular, we find that the measured Nusselt number Nu (dimensionless heat flux), as a function of Ra for water (Pr = 4.4), is well described by the power law $\mathrm{Nu} = 0.278\,\mathrm{Ra}^{0.275}$, which is consistent with the results obtained in the $\Gamma = 1$ upright cylinders with a fully developed 3D bulk flow in the studied Ra range [5].

III. EXPERIMENTAL RESULTS

A. Measurements of the mean temperature profile $\theta(z)$

Even in this confined space, we observe a well-developed thermal BL. Figure 2 shows the measured mean temperature profile $\langle T(z)\rangle$ as a function of distance z away from the bottom conducting plate for water (Pr = 4.4) at Ra = 4.23×10^9. The vertical red line indicates the thermal BL thickness δ, which is determined by the distance at which the tangent of the mean-temperature profile $\langle T(z)\rangle$ near the conducting plate intersects the bulk fluid temperature [5]. With the measured temperature of the bottom plate T_b and that at the cell center T_0, we obtain the temperature difference across the BL, $\Delta_b = T_b - T_0$, and the normalized mean temperature profile $\theta(z) = [T_b - \langle T(z)\rangle]/\Delta_b$.

Figure 3(a) shows the measured $\theta(z)$ as a function of z/δ for different values of Ra and at fixed Pr = 4.4 (water). All of the measured $\theta(z)$ curves collapse onto a single master curve once z is normalized by the BL thickness δ. The measured $\theta(z/\delta)$ thus has a universal form independent of Ra. The universal behavior of the measured $\theta(z/\delta)$ has been reported in previous experiments and DNS studies with Ra in the range $10^8 \lesssim \mathrm{Ra} \lesssim 10^{12}$ [14–28]. The different finding here is that the functional form of the measured $\theta(z/\delta)$ is well described by the calculated $\theta(\xi; c)$ using Eq. (1) with $c = 1.8$ (solid line). Similarly, Fig. 3(b) shows the measured $\theta(z)$ as a function of z/δ for different values of Ra and at fixed Pr = 7.6 (20 wt.% aqueous solution of glycerin). The functional form of the measured $\theta(z/\delta)$ is also found to be well described by Eq. (1) with $c = 2.1$ (solid line), which deviates from the PBP form (dashed line) in the region $0.6 \lesssim \xi \lesssim 2$.

Table I gives a summary of the fitted values of c obtained in different convection cells filled with a fluid of different values of Pr. As c increases ($c > 1$), a monotonically decreases, leading to a decreasing turbulent diffusivity $\kappa_t \simeq a^3\xi^3\kappa$ inside the BL. Therefore, a larger value of c indicates a smaller effect from BL fluctuations and the corresponding $\theta(z)$ becomes closer to the PBP form. As shown in Table I, the thermal BL in the thin disk with a larger value of Pr has a larger value of c,

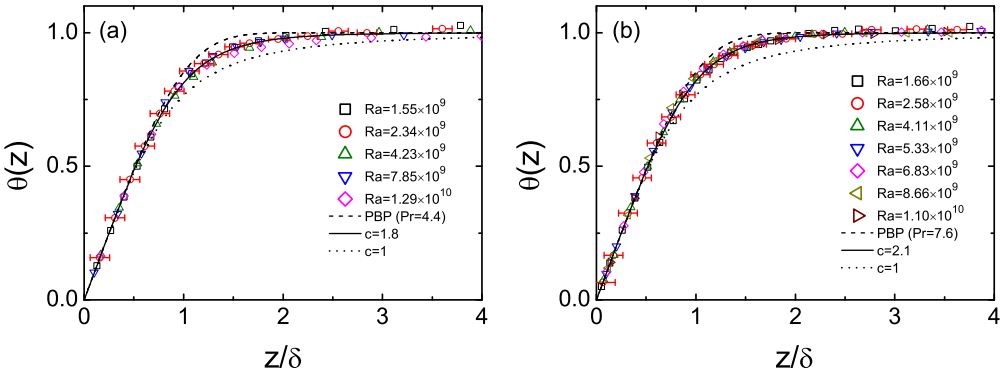

FIG. 3. (a) Normalized mean temperature profile $\theta(z)$ as a function of z/δ for different values of Ra and at fixed Pr $= 4.4$ (water). The measurements are made along the central axis of the cell near its bottom plate. The error bars indicate the size of the thermistor bead used. The solid and dotted lines are, respectively, the calculated $\theta(\xi; c)$ using Eq. (1) with $c = 1.8$ and $c = 1$. The dashed line shows the PBP profile for Pr $= 4.4$. (b) Measured $\theta(z)$ as a function of z/δ for different values of Ra and at fixed Pr $= 7.6$ (20 wt.% aqueous solution of glycerin). The solid and dotted lines are, respectively the calculated $\theta(\xi; c)$ using Eq. (1) with $c = 2.1$ and $c = 1$. The dashed line shows the PBP profile for Pr $= 7.6$.

because it is more stable and has fewer BL fluctuations. Table I also reveals an interesting effect of cell geometry. Compared to the quasi-2D flow in the thin disk, the large-scale flow in the cylinder has more fluctuations and a stronger effect on $\theta(\xi)$, making it deviate more from the PBP form (see dotted lines in Fig. 3).

B. Measurements of the temperature variance profile $\eta(z)$

While the deviations of the measured $\theta(z)$ from the PBP form are clearly visible, they are nonetheless small and are only shown in the region $0.6 \lesssim \xi \lesssim 2$. The temperature variance profile $\eta(z)$, on the other hand, is a direct measure of BL fluctuations and is absent in laminar BLs without fluctuations. Figure 4(a) shows the measured $\eta(z)$ as a function of distance z for different values of Ra and at fixed Pr $= 7.6$. In the plot, $\eta(z)$ is normalized by its maximal value η_0 and z is normalized by δ. In the region $\xi = z/\delta \lesssim 2$, all the measured $\eta(z)/\eta_0$ curves collapse onto a single master curve, which has a single peak at $\xi_0 \simeq 0.78 \pm 0.05$. A similar single-peaked $\eta(z)$ was also found in the upright cylinders [14,15,17] and rectangular cells [20]. Beyond $\xi \gtrsim 2$, the measured $\eta(z)/\eta_0$ does not scale with z/δ anymore. Instead, it scales with z/D as shown in Fig. 4(b). It can be seen that all the measured $\eta(z)/\eta_0$ curves superimpose with each other in the region $0.008 \lesssim z/D \lesssim 0.15$. Figure 4 thus reveals that the self-similar behavior of the thermal BLs remains only up to $\xi \lesssim \xi_c = z_c/\delta \simeq 2$ along the cell axis and there is a sharp transition to a new scaling regime (mixing zone) at $\xi_c \simeq 2$ (or equivalently $z_c/D \simeq 0.008$), beyond which a different theoretical model is needed [43,44].

TABLE I. Fitted values of c in Eq. (1), which are obtained in this experiment (disk) and from recent DNSs (cylinder) [33].

Sample	Pr	c
disk	4.4	1.8
disk	7.6	2.1
cylinder	4.38	1
cylinder	2547.9	2

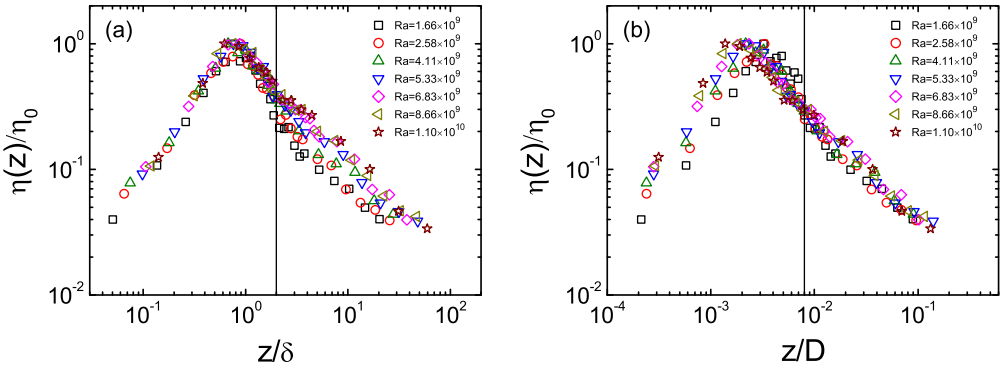

FIG. 4. Normalized temperature variance profile $\eta(z)/\eta_0$ as a function of the normalized distance (a) z/δ and (b) z/D. The measurements are made near the lower conducting plate for different values of Ra and at fixed Pr = 7.6. The vertical lines in (a) and (b) indicate the transition distance $\xi_c = (z/\delta)_c \simeq 2$ or equivalently $z/D \simeq 0.008$.

IV. THEORETICAL ANALYSIS

The scaling behavior of the measured $\eta(z)/\eta_0$ is a unique property of the thermal BLs in RBC and one has not yet found an equation to describe the function form of $\eta(z)/\eta_0$. Based on the above experimental results, we now derive an equation for $\eta(z)/\eta_0$. We consider a 2D convective flow over an infinite horizontal plate, which is governed by the convective heat equation

$$\partial_t T + \boldsymbol{V}\cdot\boldsymbol{\nabla} T = \kappa\nabla^2 T, \tag{2}$$

where $\boldsymbol{V} = u(x,z,t)\boldsymbol{e}_x + v(x,z,t)\boldsymbol{e}_z$ is the velocity field and $T(x,z,t)$ is the temperature field. In addition, $\boldsymbol{\nabla} = \boldsymbol{e}_x\partial_x + \boldsymbol{e}_z\partial_z$ and $\nabla^2 = \partial_x^2 + \partial_z^2$ are, respectively, the gradient and Laplacian operators in two dimensions. With the Reynolds decomposition

$$\boldsymbol{V}(x,z,t) = \langle \boldsymbol{V}(x,z)\rangle + \boldsymbol{V}'(x,z,t), \quad T(x,z,t) = \langle T(x,z)\rangle + T'(x,z,t) \tag{3}$$

and taking a time average $\langle\cdots\rangle$, we find

$$\langle \boldsymbol{V}\rangle\cdot\boldsymbol{\nabla}\langle T\rangle + \boldsymbol{\nabla}\cdot\langle \boldsymbol{V}'T'\rangle = \kappa\nabla^2\langle T\rangle. \tag{4}$$

Subtracting Eq. (4) from Eq. (2), multiplying by T', and taking a time average, one obtains [45]

$$\eta_0\langle \boldsymbol{V}\rangle\cdot\boldsymbol{\nabla}\Omega + 2\langle T'\boldsymbol{V}'\rangle\cdot\boldsymbol{\nabla}\langle T\rangle + \boldsymbol{\nabla}\cdot\langle \boldsymbol{V}'T'^2\rangle = \kappa\eta_0\nabla^2\Omega - 2\epsilon_T, \tag{5}$$

where $\eta(x,z) \equiv \langle T'^2(x,z)\rangle$, $\Omega(x,z) \equiv \eta(x,z)/\eta_0$, and $\epsilon_T(x,z) \equiv \kappa\langle(\boldsymbol{\nabla}T')^2\rangle$. To obtain Eq. (5), one has assumed $\partial_t\langle T'^2\rangle = 0$ for a steady-state flow and $\boldsymbol{\nabla}\cdot\boldsymbol{V}' = 0$ for an incompressible fluid. Using the BL approximations $\partial_x\langle T\rangle \ll \partial_z\langle T\rangle$, $\partial_x\langle u'T'^2\rangle \ll \partial_z\langle v'T'^2\rangle$, and $\partial_x^2\eta \ll \partial_z^2\eta$, Eq. (5) can be written as

$$\eta_0(\langle u\rangle\partial_x\Omega + \langle v\rangle\partial_z\Omega) + 2\langle T'v'\rangle\partial_z\langle T\rangle + \partial_z\langle v'T'^2\rangle = \kappa\eta_0\partial_z^2\Omega - 2\epsilon_T, \tag{6}$$

where $\epsilon_T(x,z) \equiv \kappa[\langle(\partial_x T')^2\rangle + \langle(\partial_z T')^2\rangle]$ is the thermal dissipation rate and the denotations of the velocity components and spatial coordinates are given in Fig. 1.

The first three terms in Eq. (6) have been solved in Ref. [33] for Pr $>$ 1. Using the scaling variable $\xi = z/\delta$ with $\delta \propto (\nu x/U_0)^{1/2}$, we have

$$\langle u\rangle\partial_x\Omega + \langle v\rangle\partial_z\Omega = -\frac{\kappa}{\delta^2}\beta\xi^2\frac{d\Omega(\xi)}{d\xi} \tag{7}$$

and

$$2\langle v'T'\rangle\partial_z\langle T\rangle = -2\kappa\frac{\Delta_b^2}{\delta^2}\frac{a^3\xi^3}{(1+a^3\xi^3)^{2c}}, \tag{8}$$

where $\beta = 3a^3(c-1)$ is a positive number and U_0 is the speed of the large-scale flow near the thermal BL. Similar to the temperature-velocity correlation function, the fourth term in Eq. (6) can be written as

$$\langle v'T'^2\rangle = -\kappa_f\partial_z\eta, \tag{9}$$

where κ_f is the turbulent diffusivity for the temperature variance. Similar to κ_t, we find $\kappa_f \simeq d\xi^3\kappa$ for small ξ, with d being a numerical constant describing the effect of BL fluctuations on Ω. The fact that both κ_t and κ_f have the same dependence on ξ indicates that BL fluctuations affect $\theta(\xi)$ and $\Omega(\xi)$ in a similar way.

The thermal dissipation rate $\epsilon_T(\xi)$ for small ξ can be derived from the spatial derivatives of the normalized two-point temperature correlation function along the z direction,

$$C_T(x,r) = \frac{\langle T'(x,z)T'(x,z+r)\rangle}{\langle T'^2(x,z)\rangle^{1/2}\langle T'^2(x,z+r)\rangle^{1/2}}, \tag{10}$$

where r is the separation between the two points along the z direction. For small values of r, one has [46]

$$C_T(x,r) \simeq 1 - \left(\frac{r}{\ell_z}\right)^2, \tag{11}$$

where ℓ_z is the Taylor microscale of temperature fluctuations in the z direction. At the limit $r \to 0$, the values of $C_T(x,r)$ and its derivatives are given by

$$\lim_{r\to 0} C_T(r) = 1, \quad \lim_{r\to 0}\partial_r C_T(r) = 0, \quad \lim_{r\to 0}\partial_r^2 C_T(r) = -\frac{2}{\ell_z^2}. \tag{12}$$

With the above equations, one has

$$\kappa\langle T'(z)\partial_z^2 T'(z)\rangle = \kappa\lim_{r\to 0}\partial_r^2\langle T'(z)T'(z+r)\rangle = \kappa\langle T'^2(z)\rangle^{1/2}\lim_{r\to 0}\partial_r^2[C_T(r)\langle T'^2(z+r)\rangle^{1/2}]. \tag{13}$$

Substituting Eqs. (12) into Eq. (13), we have

$$\kappa\langle T'(z)\partial_z^2 T'(z)\rangle = \kappa\left[\frac{1}{2}\partial_z^2\eta - \frac{1}{4}\frac{(\partial_z\eta)^2}{\eta} - \frac{2\eta}{\ell_z^2}\right]. \tag{14}$$

Note that

$$\kappa\langle T'(z)\partial_z^2 T'(z)\rangle = \kappa\left[\tfrac{1}{2}\partial_z^2\eta - \langle(\partial_z T')^2\rangle\right]. \tag{15}$$

Substituting Eq. (15) into Eq. (14), we have

$$\kappa\langle(\partial_z T')^2\rangle = \kappa\left[\frac{1}{4}\frac{(\partial_z\eta)^2}{\eta} + \frac{2\eta}{\ell_z^2}\right]. \tag{16}$$

Similarly, from $\kappa\langle\delta T\partial_x^2\delta T\rangle$ we can derive

$$\kappa\langle(\partial_x T')^2\rangle = \kappa\left[\frac{1}{4}\frac{(\partial_x\eta)^2}{\eta} + \frac{2\eta}{\ell_x^2}\right], \tag{17}$$

where ℓ_x is the Taylor microscale of temperature fluctuations in the x direction. Using the BL approximation $|\partial_x\eta| \ll |\partial_z\eta|$ and the scaling variable ξ, we obtain the thermal dissipation rate $\epsilon_T(\xi)$

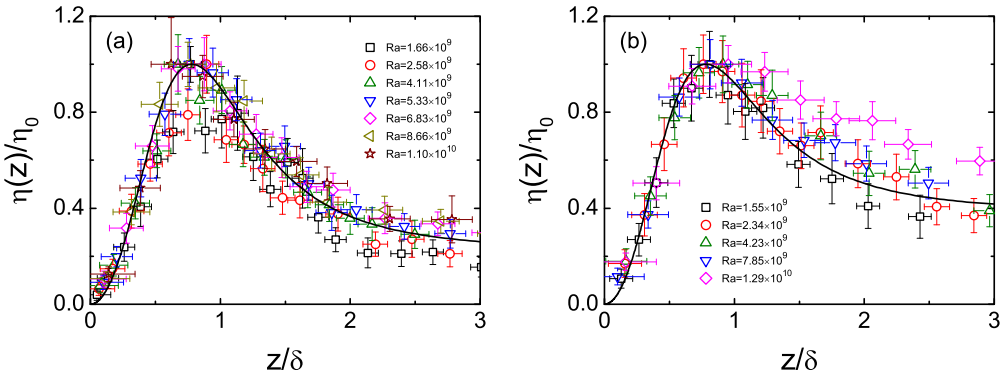

FIG. 5. (a) Measured temperature variance profile $\eta(z)/\eta_0$ as a function of the normalized distance z/δ for different values of Ra and at fixed Pr = 7.6 (glycerin solution). The data are the same as those shown in Fig. 4(a) but are plotted on the linear scale for a clearer view of the fitting. The solid curve shows the numerical solution $\Omega(\xi;2.1,68,2.2,1)$ of Eq. (20). (b) Measured $\eta(z)/\eta_0$ as a function of z/δ for different values of Ra and at fixed Pr = 4.4 (water). The solid line shows the numerical solution $\Omega(\xi;1.8,62,3.35,1.35)$ of Eq. (20) with $\xi_0 = 0.78$.

from Eqs. (16) and (17),

$$\epsilon_T(\xi) \equiv \kappa\langle[\nabla T'(\xi)]^2\rangle = \kappa\frac{\eta_0}{\delta^2}\left(\frac{1}{4}\frac{[d\Omega(\xi)/d\xi]^2}{\Omega(\xi)} + \alpha\Omega(\xi)\right), \tag{18}$$

where

$$\alpha = 2\delta^2\left(\frac{1}{\ell_x^2} + \frac{1}{\ell_z^2}\right). \tag{19}$$

By substituting Eqs. (7)–(9) and Eq. (18) into Eq. (6), we have

$$(1+d\xi^3)\frac{d^2\Omega(\xi)}{d\xi^2} + (\beta+3d)\xi^2\frac{d\Omega(\xi)}{d\xi} + 2\frac{\Delta_b^2}{\eta_0}\frac{a^3\xi^3}{(1+a^3\xi^3)^{2c}} - \frac{1}{2}\frac{[d\Omega(\xi)/d\xi]^2}{\Omega(\xi)} - 2\alpha\Omega(\xi) = 0 \tag{20}$$

and the initial conditions of $\Omega(\xi)$ are

$$\Omega(\xi_0) = 1, \quad \frac{d\Omega(\xi_0)}{d\xi} = 0. \tag{21}$$

Here ξ_0 (=0.78) is the peak position of $\Omega(\xi)$, as shown in Fig. 4(a). Equation (20) is an ordinary differential equation, which can be numerically solved using the Runge-Kutta method under the initial conditions given in Eq. (21).

The final solution $\Omega(\xi;c,\Delta_b^2/\eta_0,d,\alpha)$ has four parameters. The parameter c has been obtained separately from the fitting of Eq. (1) to the measured $\theta(z)$, as shown in Fig. 3. The parameter Δ_b^2/η_0 is a measurable quantity, which is directly determined from the experiment. There are only two adjustable parameters remaining, d and α, which are used to best fit the measured $\eta(z)/\eta_0$. Figure 5(a) shows a comparison between the numerical solution $\Omega(\xi;2.1,68,2.2,1)$ of Eq. (20) (solid line) and the measured $\eta(z)/\eta_0$ in the range $\xi \lesssim 3$, which is obtained for Pr = 7.6. Excellent agreement is obtained between the theory and experimental data. An equally good fitting is also obtained between the numerical solution $\Omega(\xi;1.8,62,3.35,1.35)$ and the experimental data with Pr = 4.4 (water), as shown in Fig. 5(b). When Pr increases, Δ_b^2/η_0 also increases (η_0 decreases) and the value of d decreases (κ_f decreases). Both trends indicate consistently that BL fluctuations are reduced and thus the BL profile becomes closer to the laminar type.

V. CONCLUSION

In this investigation we derive a BL equation [Eq. (20)] for the temperature variance profile $\eta(z)$. This equation, together with Eq. (1) for the mean temperature profile $\theta(z)$ [33], provides a unique theoretical framework with a common set of parameters to quantitatively describe the effect of BL fluctuations. The simultaneously measured $\theta(z)$ and $\eta(z)$ in a specially designed quasi-2D convection cell verify the theoretical predictions. The experimental results demonstrate that the effect of BL fluctuations can indeed be described by the velocity-temperature correlation functions and our BL equations capture the essential physics. This work not only is useful for the understanding of BL fluctuations in turbulent thermal convection, but is also relevant to many practical applications in wall-bounded turbulent flows.

ACKNOWLEDGMENTS

We thank E. Ching for useful discussions. This work was supported by RGC of Hong Kong SAR under Grant No. C6004-14G (P.T.). X.H. acknowledges support through the China Thousand Young Talents Program.

[1] F. H. Busse, Convection driven zonal flows and vortices in the major planets, Chaos **4**, 123 (1994).
[2] E. D. Siggia, High Rayleigh number convection, Annu. Rev. Fluid Mech. **26**, 137 (1994).
[3] L. P. Kadanoff, Turbulent heat flow: Structures and scaling, Phys. Today **54**(8), 34 (2001).
[4] E. van Doorn, B. Dhruva, K. R. Sreenivasan, and V. Cassella, Statistics of wind direction and its increments, Phys. Fluids **12**, 1529 (2000).
[5] G. Ahlers, S. Grossmann, and D. Lohse, Heat transfer and large scale dynamics in turbulent Rayleigh-Bénard convection, Rev. Mod. Phys. **81**, 503 (2009).
[6] F. Chillà and J. Schumacher, New perspectives in turbulent Rayleigh-Bénard convection, Eur. Phys. J. E **35**, 58 (2012).
[7] S. Grossmann and D. Lohse, Scaling in thermal convection: A unifying theory, J. Fluid Mech. **407**, 27 (2000).
[8] L. D. Landau and E. M. Lifshitz, *Fluid Mechanics*, 2nd ed., Course of Theoretical Physics (Pergamon, Oxford, 1987), Vol. 6.
[9] H. Schlichting and K. Gersten, *Boundary Layer Theory*, 8th ed. (Springer, Berlin, 2000).
[10] R. H. Kraichnan, Turbulent thermal convection at arbitrary Prandtl number, Phys. Fluids **5**, 1374 (1962).
[11] E. A. Spiegel, Convection in stars, Annu. Rev. Astron. Astrophys. **9**, 323 (1971).
[12] B. I. Shraiman and E. D. Siggia, Heat transport in high-Rayleigh-number convection, Phys. Rev. A **42**, 3650 (1990).
[13] S. Grossmann and D. Lohse, Multiple scaling in the ultimate regime of thermal convection, Phys. Fluids **23**, 045108 (2011).
[14] A. Belmonte, A. Tilgner, and A. Libchaber, Boundary Layer Length Scales in Thermal Turbulence, Phys. Rev. Lett. **70**, 4067 (1993).
[15] A. Belmonte, A. Tilgner, and A. Libchaber, Temperature and velocity boundary layers in turbulent convection, Phys. Rev. E **50**, 269 (1994).
[16] S.-L. Lui and K.-Q. Xia, Spatial structure of the thermal boundary layer in turbulent convection, Phys. Rev. E **57**, 5494 (1998).
[17] Y.-B. Du and P. Tong, Turbulent thermal convection in a cell with ordered rough boundaries, J. Fluid Mech. **407**, 57 (2000).
[18] R. J. A. M. Stevens, Q. Zhou, S. Grossmann, R. Verzicco, K.-Q. Xia, and D. Lohse, Thermal boundary layer profiles in turbulent Rayleigh-Bénard convection in a cylindrical sample, Phys. Rev. E **85**, 027301 (2012).

[19] R. du Puits, C. Resagk, and A. Thess, Thermal boundary layers in turbulent Rayleigh-Bénard convection at aspect ratios between 1 and 9, New J. Phys. **15**, 013040 (2013).
[20] Q. Zhou and K.-Q. Xia, Thermal boundary layer structure in turbulent Rayleigh-Bénard convection in a rectangular cell, J. Fluid Mech. **721**, 199 (2013).
[21] M. van Reeuwijk, H. J. J. Jonker, and K. Hanjalić, Wind and boundary layers in Rayleigh-Bénard convection. II. Boundary layer character and scaling, Phys. Rev. E **77**, 036312 (2008).
[22] R. J. A. M. Stevens, R. Verzicco, and D. Lohse, Radial boundary layer structure and Nusselt number in Rayleigh-Bénard convection, J. Fluid Mech. **643**, 495 (2010).
[23] N. Shi, M. S. Emran, and J. Schumacher, Boundary layer structure in turbulent Rayleigh-Bénard convection, J. Fluid Mech. **706**, 5 (2012).
[24] S. Wagner, O. Shishkina, and C. Wagner, Boundary layers and wind in cylindrical Rayleigh-Bénard cells, J. Fluid Mech. **697**, 336 (2012).
[25] J. D. Scheel, E. Kim, and K. R. White, Thermal and viscous boundary layers in turbulent Rayleigh-Bénard convection, J. Fluid Mech. **711**, 281 (2012).
[26] O. Shishkina, S. Horn, and S. Wagner, Falkner-Skan boundary layer approximation in Rayleigh-Bénard convection, J. Fluid Mech. **730**, 442 (2013).
[27] J. D. Scheel and J. Schumacher, Local boundary layer scales in turbulent Rayleigh-Bénard convection, J. Fluid Mech. **758**, 344 (2014).
[28] J. Wang and K.-Q. Xia, Spatial variations of the mean and statistical quantities in the thermal boundary layers of turbulent convection, Eur. Phys. J. B **32**, 127 (2003).
[29] Q. Zhou and K.-Q. Xia, Measured Instantaneous Viscous Boundary Layer in Turbulent Rayleigh-Bénard Convection, Phys. Rev. Lett. **104**, 104301 (2010).
[30] G. Ahlers, E. Bodenschatz, D. Funfschilling, S. Grossmann, X. He, D. Lohse, R. Stevens, and R. Verzicco, Logarithmic Temperature Profiles in Turbulent Rayleigh-Bénard Convection, Phys. Rev. Lett. **109**, 114501 (2012).
[31] G. Ahlers, E. Bodenschatz, and X. He, Logarithmic temperature profiles of turbulent Rayleigh-Bénard convection in the classical and ultimate state for a Prandtl number of 0.8, J. Fluid Mech. **758**, 436 (2014).
[32] P. Wei and G. Ahlers, Logarithmic temperature profiles in the bulk of turbulent Rayleigh–Bénard convection for a Prandtl number of 12.3, J. Fluid Mech. **758**, 809 (2014).
[33] O. Shishkina, S. Horn, S. Wagner, and E. S. C. Ching, Thermal Boundary Layer Equation for Turbulent Rayleigh-Bénard Convection, Phys. Rev. Lett. **114**, 114302 (2015).
[34] E. Brown and G. Ahlers, Azimuthal asymmetries of the large-scale circulation in turbulent Rayleigh-Bénard convection, Phys. Fluids **20**, 105105 (2008).
[35] H.-D. Xi, S.-Q. Zhou, Q. Zhou, T.-S. Chan, and K.-Q. Xia, Origin of the Temperature Oscillation in Turbulent Thermal Convection, Phys. Rev. Lett. **102**, 044503 (2009).
[36] E. Brown and G. Ahlers, The origin of oscillations of the large-scale circulation of turbulent Rayleigh-Bénard convection, J. Fluid Mech. **638**, 383 (2009).
[37] C. Sun, K-Q. Xia, and P. Tong, Three-dimensional flow structures and dynamics of turbulent thermal convection in a cylindrical cell, Phys. Rev. E **72**, 026302 (2005).
[38] F. F. Araujo, S. Grossmann, and D. Lohse, Wind Reversals in Turbulent Rayleigh-Bénard Convection, Phys. Rev. Lett. **95**, 084502 (2005).
[39] K. Sugiyama, R. Ni, R. J. A. M. Stevens, T.-S. Chan, S.-Q. Zhou, H.-D. Xi, C. Sun, S. Grossmann, K.-Q. Xia, and D. Lohse, Flow Reversals in Thermally Driven Turbulence, Phys. Rev. Lett. **105**, 034503 (2010).
[40] H. Song, E. Villermaux, and P. Tong, Coherent Oscillations of Turbulent Rayleigh-Bénard Convection in a Thin Vertical Disk, Phys. Rev. Lett. **106**, 184504 (2011).
[41] X. He and P. Tong, Measurements of the thermal dissipation field in turbulent Rayleigh-Bénard convection, Phys. Rev. E **79**, 026306 (2009).
[42] H. Song, E. Brown, R. Hawkins, and P. Tong, Dynamics of large-scale circulation of turbulent thermal convection in a horizontal cylinder, J. Fluid Mech. **740**, 136 (2014).
[43] B. Castaing, G. Gunaratne, F. Heslot, L. Kadanoff, A. Libchaber, S. Thomae, X.-Z. Wu, S. Zaleski, and G. Zanetti, Scaling of hard thermal turbulence in Rayleigh-Bénard convection, J. Fluid Mech. **204**, 1 (1989).

[44] R. J. Adrian, Variation of temperature and velocity fluctuations in turbulent thermal convection over horizontal surfaces, Int. J. Heat Mass Transfer **39**, 2303 (1996).

[45] B. E. Launder, in *Topics in Applied Physics 12: Turbulence*, edited by P. Bradshaw (Springer, Berlin, 1976), Chap. 6, pp. 231–287.

[46] X. He, G.-W. He, and P. Tong, Small-scale turbulent fluctuations beyond Taylors frozen-flow hypothesis, Phys. Rev. E **81**, 065303(R) (2010).